

On the Stability of Robot Compliant Motion Control: Theory and Experiments

H. Kazerooni

B. J. Waibel

S. Kim

Mechanical Engineering Department,
University of Minnesota,
Minneapolis, MN 55455

The work presented here is a nonlinear approach for the stability analysis of robot manipulators in compliant maneuvers. Stability of the environment and the manipulator taken as a whole has been investigated, and a bound for stable manipulation has been derived. The stability analysis has been investigated using unstructured models for the dynamic behavior of the robot manipulator and the environment. This unified approach of modeling robot dynamics is expressed in terms of sensitivity functions as opposed to the rigid body dynamics derived by Lagrangian approach. It allows us to incorporate the dynamic behavior of all the elements of a robot manipulator (i.e., actuators, sensors and the structural compliance of the links) in addition to the rigid body dynamics. We show that for stability of the robot, there must be some initial compliancy either in the robot or in the environment. According to this stability condition, smaller sensitivity either in the robot or in the environment leads to a narrower stability range. In the limit, when both robot and environment have zero sensitivity, stability cannot be guaranteed. The general stability condition has been extended to the particular case where the environment is very rigid in comparison with the robot stiffness. This condition has been verified via simulation and experiment on the Minnesota direct drive robot.

1 Introduction

Most assembly operations and manufacturing tasks require mechanical interactions with the environment or with the object being manipulated, along with "fast" motion in unconstrained space. Robotic deburring [7] is an example of such tasks. In constrained maneuvers, the interaction force¹ must be accommodated rather than resisted. Two methods have been suggested for development of compliant motion. The first method is aimed at controlling force and position in a nonconflicting way [16, 17, 18, 24]. In this approach, force is commanded along those directions constrained by the environment, while position is commanded along those directions in which the manipulator is unconstrained and free to move. The second method is focused on developing a relationship between the interaction force and the manipulator position [3, 4, 5, 8, 11, 12, 13, 19]. By controlling the manipulator position and specifying its relationship with the interaction force, a designer can ensure that the manipulator will be able to maneuver in a constrained space while maintaining appropriate contact force. This paper describes an analysis on the stability of the robot and environment taken as a whole when the second method is employed to control the robot

compliance. The stability of the robotic constrained maneuvers has been reported in references [1, 5, 8, 13]; a stability condition for a linear single degree of freedom system has been described in references [1 and 3].

The objective is to arrive at some building blocks for stability of robot constrained maneuvers. We choose unstructured modeling for the interaction of the robot and environment in their most general forms. These models do not have any particular structure, yet they can model a wide variety of industrial and research robot manipulators and environment dynamic behavior. Although this approach of modeling may not lead to any design procedure, it will allow us to understand the fundamental issues in stability when a robot interacts with an environment. Using structured modeling and control leads to a special stability condition that cannot be applied to a general class of problems. We also believe choosing particular transfer functions to model various components of the robot (e.g., motors and link stiffness) fail to yield general solution, yet they give insights into the general problem. In section two we bring up an example to show how unstructured modeling applies to structured systems. This example is given here to illustrate the guiding principle of the more general theory presented later and is *not* intended to be a general analysis of robot and environment dynamics.

Sections 3 and 4 are dedicated to unstructured modeling, control and stability analysis. Using unstructured models for the robot and environment, we analyze the stability of the robot and environment via the Small Gain Theorem and Nyquist Criterion. We show that the stability criterion derived via

¹In this article, "force" implies force and torque, and "position" implies position and orientation.

Contributed by the Dynamic Systems and Control Division for publication in the JOURNAL OF DYNAMIC SYSTEMS, MEASUREMENT AND CONTROL. Manuscript received by the Dynamic Systems and Control Division August 1988; revised manuscript received March 1989. Associate Editor: R. Shoureshi.

the Nyquist method is a subclass of the condition derived by the Small Gain Theorem. For a particular application, one can replace the unstructured dynamic models with known models and then a tighter condition can be achieved. The stability criterion reveals that there must be some initial compliancy either in the robot or in the environment. The initial compliancy in the robot can be obtained by a passive compliant element such as an RCC (Remote Center Compliance) or compliancy within the positioning feedback. Practitioners always observed that the system of a robot and a stiff environment can always be stabilized when a compliant element (e.g., piece of rubber or an RCC) is installed between the robot and environment. The stability criterion also shows that no compensator can be found to stabilize the interaction of the ideal positioning system (very rigid tracking robot) with an infinitely rigid environment. In this case the robot and environment both resemble ideal sources of flow (defined in bond graph theory) and they do not physically complement each other. Sections 5 and 6 confine the control and stability analysis to direct drive robots where rigid body dynamics have been employed to develop structured dynamic equations for robot behavior. The stability condition has been verified on the Minnesota robot via simulation and experiment in Section 7.

2 Motivation

Throughout this paper, we analyze manipulators using unstructured dynamic models which focus on the device's input-output relationships rather than a particular dynamic structure. Although the framework of unstructured models leads to general conclusions, a given robot's dynamics are typically characterized by a structured model. In this section, we show, through a simple, one-dimensional manipulator modeled by linear transfer functions, how a structured model can be applied within the general analysis that follows. Moreover, this example typifies the approach used in analyzing a multivariable and nonlinear robotic systems, where input-output relationships may represent nonlinear mappings rather than transfer functions.

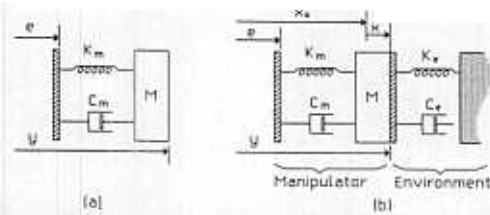


Fig. 1(a) Manipulator performing unconstrained motions under PD control

Fig. 1(b) Manipulator performing constrained motion and deflecting the environment by x

Consider the model for a one-dimensional manipulator shown in Fig. 1(a), where the command position is given by e and the actual robot position is given by y . This system consists of a point mass, M , whose trajectory is under PD (proportional plus derivative) control. The passive elements, K_m and C_m , in the model represent the position and velocity gains of the controller; these components arise due to the electronic controller—there are no passive components in the physical system. This model represents a robot manipulator with a position controller, so as K_m and C_m are increased, the bandwidth of the closed loop robot controller becomes larger, yielding faster response. In the limit, when K_m and C_m approach infinity, the closed loop controller approaches infinite bandwidth. If the position of M and the command position, e , are expressed relative to a nonmoving coordinate frame, the dynamic equation for the system is:

$$M\ddot{y} + C_m\dot{y} + K_m y = K_m e + C_m \dot{e} \quad (1)$$

Figure 1(b) shows the manipulator interacting with an environment modeled as a spring and dashpot. This model is not intended to be a general structure for the environmental dynamics. It is a simple representative model of many practical situations. The dynamics of the two interacting systems are characterized by:

Nomenclature

A = the closed-loop mapping r to e in Fig. 4	H = compensator (operating on the contact force, f)	V = the forward loop mapping from e to f in Fig. 4
$C[\theta, \dot{\theta}]$ = robot coriolis and centrifugal forces	I_n = identity matrix	x = vector of the environment deflection
D = damping matrix for linearly treated environment	I = inertia matrix for linearly treated environment	y = vector of the robot end-point position
d = vector of the external force on the robot end-point ²	J = Jacobian	y_∞ = the limiting value of the robot position for infinitely rigid environment
e = input trajectory vector	r = input-command vector	x_0 = vector of the environment position before contact
E = environment dynamics	K = stiffness matrix for linearly treated environment	θ = vector of the joint angles of the robot
f = vector of the contact force, $[f_1, f_2, \dots, f_n]^T$	K_p and K_v = position and velocity feedback gain	θ_d = command vector in the joint angles coordinate frame
f_∞ = the limiting value of the contact force for infinitely rigid environment	$M[\theta]$ = robot inertia matrix	$\epsilon_e, \epsilon_d, \mu, \gamma$ = positive scalars
G = robot dynamics with positioning controller	n = degrees of the freedom of the robot $n \leq 6$	ω_0 = bandwidth of G
	S = robot manipulator sensitivity (1/stiffness)	
	T = positive scalar	
	τ = robot joint torques	

²Unless otherwise noted, all vectors in this paper are $n \times 1$ and all matrices are $n \times n$, where n is the number of degrees of freedom in the manipulator.

$$M\ddot{y} + C_m\dot{y} + K_m y = K_m e + C_m \dot{e} + d \quad (2)$$

$$d = -f \quad (3)$$

$$f = K_e x + C_e \dot{x}, \quad \text{where } x = y - x_0 \quad (4)$$

where K_e and C_e are the stiffness and damping of the environment and x_0 is the location of the environment surface before deformation occurs. d is the force imposed on the robot while f represents the force on the environment. The condition $y - x_0 \geq 0$ indicates that the environment can bear forces only in the "pushing" direction, i.e., the contact forces must be compressive. If $y - x_0 < 0$, the manipulator's dynamics are given by equation (1). Using Laplace operator, equations (2), (3), and (4) can be represented by equations (5), (6), (7) in frequency domain.

$$y(s) = \frac{sC_m + K_m}{Ms^2 + C_m s + K_m} e(s) + \frac{1}{Ms^2 + C_m s + K_m} d(s) \quad (5)$$

$$d(s) = -f(s) \quad (6)$$

$$f(s) = (K_e + sC_e)x(s) \quad (7)$$

Given equations (5), (6), and (7), the position transfer function, $G(s)$, the sensitivity transfer function, $S(s)$, and the environment transfer function, $E(s)$ can be straightforwardly determined.

$$y(s) = G(s)e(s) + S(s)d(s) \quad (8)$$

$$f(s) = E(s)x(s) \quad (9)$$

$$G(s) = \frac{sC_m + K_m}{Ms^2 + C_m s + K_m}, \quad S(s) = \frac{1}{Ms^2 + C_m s + K_m},$$

and $E(s) = (K_e + sC_e)$.

$G(s)$ represents the transfer function from the command position, e , to the actual position, y , when the manipulator is performing unconstrained maneuvers. The manipulator's sensitivity physically represents the relationship between the force acting on the manipulator, d , and y when the command position, e , is zero. Lastly, the transfer function of the environment, E , is the relationship between the environment deflection and the contact force acting on the environment.

We use the above example to state that the end-point position of a robot with a positioning controller in general, is function of its input command and the external forces. In constrained maneuvers, these external forces are functions of the environment dynamics. Although in this example we arrived at second order transfer functions for $G(s)$ and $S(s)$, it is possible that in a more complex system, the dynamics cannot be modeled by second order relationships, such as equations (1) and (2). Throughout the remainder of this paper, we concentrate on the unstructured approach indicated by equations (8) and (9) which can be used for any linear, one-dimensional system and generalize this approach for application to multivariable and nonlinear manipulators. Hence, we analyze the system using a generalized form of the G and S relationships and assume that, in application, they can be obtained from the applicable manipulator model.

3 Unstructured Modeling

Given the motivation for an unstructured modeling, we now return to generalize equations (8) and (9) to represent the input-output mappings of the manipulator and the environment.

The end-point position of a robot manipulator that has a positioning controller is a dynamic function of both its input

trajectory vector, e , and the external force, d . The structure of the positioning controller is not of importance in this analysis, however references [2, 23] give detailed description for development of tracking systems for robot manipulators. Let G and S be two functions that show the robot end-point position in a global coordinate frame, y , is a function of the input trajectory, e , and the external force, d .³

$$y = G(e) + S(d) \quad (10)$$

The motion of the robot end-point in response to imposed forces, d , is caused by either structural compliance in the robot or by the compliance of the positioning controller, as illustrated in the example. In a simple example, if a Remote Center Compliance (RCC) with a linear dynamic behavior is installed at the end-point of the robot, then S is equal to the reciprocal of stiffness (impedance in the dynamic sense) of the RCC. S is called the sensitivity function, and it maps the external forces to the robot position. Robot manipulators with good positioning capability are characterized by S having a small gain. Whenever an external force is applied to the robot, the end-point of the robot arm will move in response. If the robot arm is a "good" positioning system, the change in position due to the external force will be "small" as long as the magnitude of the external force lies within certain limits. The sensitivity function S is defined as a mapping from the externally applied force vector to the resulting position vector for the robot arm. There is no restriction on the form of the mapping, S —it may be a linear or nonlinear⁴.

Similarly, the environment can be considered from the viewpoint of an unstructured model. If one point on the environment is displaced as vector of x , with force vector, f , then the dynamic behavior of the environment is given by equation (11).

$$f = E(x) \quad (11)$$

This equation represents a general mapping from x to f . For the purposes of our analysis, it is convenient to consider E to be an odd function; however, in physical application, f may be zero if x is negative. For example, in the grinding of a surface, the robot can only push the surface. If one considers positive f_i for "pushing" and negative f_i for "pulling," in this class of manipulation, the robot manipulator and the environment are in contact with each other only along those directions where $f_i > 0$ for $i = 1, \dots, n$. In some applications such as turning a bolt, the interaction force can be either positive or negative, meaning that the interaction torque can be clockwise or counter-clockwise. The nonlinear discriminator block diagram in Fig. 2 is drawn with a dashed line to represent the above concept—the block is present when the interaction forces can only be compressive. One can consider the truth of equation

³The assumption that linear superposition (in equation (10)) holds for the effects of d and e is useful in understanding the nature of the interaction between the robot and the environment. This interaction is in a feedback form and will be clarified with the help of Fig. 2. We will note later that the results of the nonlinear analysis do not depend on this assumption, and one can extend the obtained results to cover the case when $G(e)$ and $S(d)$ are not additive.

⁴The readers can refer to Fig. 7 to observe one possible example of internal structure of the model represented by equation (10). This figure has been employed to depict the internal structure of the Minnesota robot tracking controller. This robot has been used for experimental verification of the stability condition. The robot open loop dynamic equation is $M(\theta)\ddot{\theta} + C(\theta, \dot{\theta})\dot{\theta} = \tau + J^T d$ where $M(\theta)$, $C(\theta, \dot{\theta})$ and J are the inertia matrix, coriolis and the Jacobian.

With the help of two mappings, $kin^{-1}(\cdot)$ and $kin(\cdot)$, we define θ_d and θ as the desired position and the actual position of the robot in the joint coordinate frame. K_p and K_v are appropriate position and velocity gains to stabilize the system [1, 2, 23]. The system in Fig. 7 with two inputs (e and d), and one output, y , can be represented by block diagram of Fig. 2. Note that equation 10 is not restricted to be composed of the elements of the block diagram of Fig. 7; the block diagram of Fig. 7 is mentioned here as an example to show how one can actually model a robot with tracking controller via equation (10).

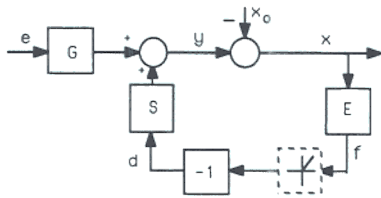


Fig. 2 The block diagram of the robot and environment. x_0 represents the environment position before contact occurs.

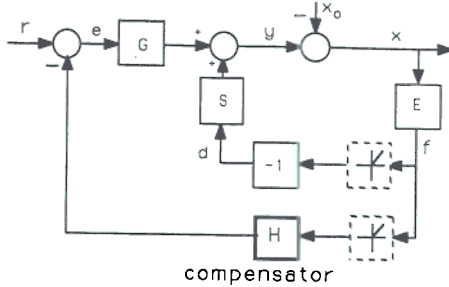


Fig. 3 Addition of a compliance compensator to the robot and environment dynamics

(11) by analyzing the relationship of the force and displacement of a spring as a simple model of the environment. E resembles the stiffness of the spring. References [11 and 12] represent $(Is^2 + Ds + K)$ for E where I , D and K are symmetric matrices and $s = j\omega$ [14]. I is the positive definite inertia matrix while D and K are the positive semidefinite damping and the stiffness matrices, respectively.

The V operator defined as a mapping from e to f and is a general relationship that encompasses the G , S , and E operators within Fig. 2. V is assumed to be a stable operator in L_p -sense; therefore $V: L_p^n \rightarrow L_p^n$ and also $\|V(e)\|_p \leq \alpha_1 \|e\|_p + \beta_1$. (See Appendix A for some definitions on L_p stability.) With this assumption, we basically claim that a robot with stable tracking controller remains stable when it is in contact with an environment. Note that one can still define V without assuming the superposition of effects of e and d in equation (10).⁵

4 Unstructured Control and Stability Analysis

Figure 3 shows the system when compliance compensator, H , is incorporated in the control structure. When the robot is not in contact with the environment (i.e., the outer feedback loops in Fig. 3 do not exist), the actual position of the robot end-point is governed by equation (10). When the robot is in contact with the environment, then the contact force follows r according to equations (10) and (11). The input command vector, r , is used differently for the two categories of maneuverings; as an input trajectory command in unconstrained space (equation (10)) and as a command to control force in constrained space. We do not command any set-point for force as we do in admittance control [16, 17, 18, 24]. This method is referred to as Impedance Control [4, 11, 12, 19] because it accepts a position vector as input and it reflects a force vector as output. There is no hardware or software switch in the control system when the robot travels between unconstrained space and constrained space. The feedback loop on the contact force

⁵For the benefit of clarity, we develop the frequency domain theory for linearly treated robots in parallel with the nonlinear analysis. The linear analysis is useful not only for analysis of robots with inherently linear dynamics, but also for robots with locally linearized dynamic behavior. In the latter case, the analysis is correct only in the neighborhood of the operating point. If G , S , and E represent linear, multivariable transfer functions, $x_0 = 0$ and the nonlinear discriminator block is omitted, V becomes a transfer function defined by:

$$V(s) = E(I_n + SE)^{-1}G$$

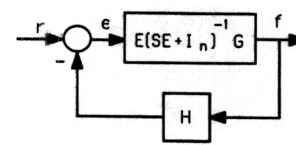


Fig. 4 Manipulator and the environment with force feedback compensator

closes naturally when the robot encounters the environment.

By knowing S , G , E , and choosing H , one can shape the contact force. The value of H is the choice of designer and, depending on the task, it can have various values in different directions.⁶ A large value for H develops a compliant robot while a small H generates a stiff robot. Reference [8] describes a micro-manipulator in which the compliance in the system is shaped for metal removal application. By closing the loop via H , one can not only add to the total sensitivity but also shape the sensitivity of the system. One cannot choose arbitrarily large values for H ; the stability of the closed-loop system of Fig. 3 must also be guaranteed.

The objective is to arrive at a sufficient condition for stability of the system shown in Fig. 3. This sufficient condition leads to the introduction of a class of compensators, H , that can be used to develop compliancy in the system of Fig. 3. Using the operator V , Fig. 4 is presented as the simplified version of Fig. 3. Since the P norm of the discriminator block diagrams (dotted line) have gains that are smaller than unity [21], then they are replaced by unity gain transfer functions.⁷ This may result in a more conservative stability condition. First, we use the Small Gain Theorem to derive the general stability condition of the block diagram of Fig. 4. Then, with the help of a corollary, we show the stability condition when H is chosen as a linear operator (transfer function matrix) while V is a nonlinear operator. The following proposition (using the Small Gain Theorem in reference [21, 22]) states the stability condition of the closed-loop system shown in Fig. 4. If conditions I, II, and III hold:

I. V is a L_p -stable operator, that is

$$a) V(e): L_p^n \rightarrow L_p^n \quad (12)$$

$$b) \|V(e)\|_p \leq \alpha_1 \|e\|_p + \beta_1 \quad (13)$$

II. H is chosen such that mapping $H(f)$ is L_p -stable, that is

$$a) H(f): L_p^n \rightarrow L_p^n \quad (14)$$

$$b) \|H(f)\|_p \leq \alpha_2 \|f\|_p + \beta_2 \quad (15)$$

$$\text{III. and } \alpha_1 \alpha_2 < 1 \quad (16)$$

then the closed-loop system (Fig. 4) is L_p -stable. The proof is given in Appendix A. Since:

$$f = V(e) \quad (17)$$

then substituting for $\|f\|_p$ from inequality (13) into inequality (15) results in inequality (18).

$$\|H(V(e))\|_p \leq \alpha_1 \alpha_2 \|e\|_p + \alpha_2 \beta_1 + \beta_2 \quad (18)$$

$\alpha_1 \alpha_2$ in inequality (18) represents the gain of the loop mapping, $H(V(e))$. The third stability condition requires that H be

⁶The contact force for the linear case is given as: $f = E(I_n + SE + GHE)^{-1}Gr$ where the environment admittance (1/impedance in the linear domain), E^{-1} , the robot sensitivity (1/stiffness in the linear domain), S , and the electronic compliancy, GH , add together to form the total compliancy of the system. If $H = 0$, then only the admittance of the environment and the robot add together to form the compliancy for the system.

⁷The describing function of this nonlinearity also has a gain smaller than unity for all frequencies.

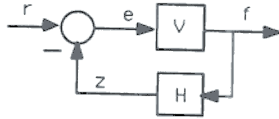


Fig. 5 The simplification of Fig. 3 when all the operators are linear transfer function matrices.

chosen such that the loop mapping, $H(V(e))$, is linearly bounded with less than a unity slope.

Corollary. If H is chosen as a linear operator (the impulse response) while the other operator is nonlinear, then:

$$\|HV(e)\|_p \leq \gamma \|V(e)\|_p \quad (19)$$

where: $\gamma = \sigma_{\max}(N)$ (20)

σ_{\max} indicates the maximum singular value,⁸ and N is the L_1 norm of each corresponding member of H . Considering inequality (19), inequality (18) can be rewritten as:

$$\|HV(e)\|_p \leq \gamma \|V(e)\|_p \leq \gamma \alpha_1 \|e\|_p + \gamma \beta_1 \quad (21)$$

Comparing inequality (21) with inequality (18), to guarantee the closed-loop stability; $\gamma \alpha_1$ must be smaller than unity, or, equivalently:

$$\gamma < \frac{1}{\alpha_1} \quad (22)$$

to guarantee the stability of the closed-loop system, H in Fig. 4 must be chosen such that its "size," as indicated by γ , is smaller than the reciprocal of the "gain" of the forward loop mapping, as indicated by α_1 .

When all the operators of Fig. 4 are linear transfer function matrices, using Multivariable Nyquist Criterion, inequality (23) can be used as a sufficient condition for stability (Appendix B).

$$\sigma_{\max}(H) < \frac{1}{\sigma_{\max}(E(I_n + SE)^{-1}G)} \text{ for all } \omega \in (0, \infty) \quad (23)$$

Similar to the nonlinear case, H must be chosen such that $\sigma_{\max}(H)$ is smaller than the reciprocal of the maximum singular value of the forward loop mapping in Fig. 5 to guarantee the stability of the closed-loop system. Appendix C shows that the linear stability condition given by inequality (23) is a subclass of the nonlinear stability condition.

To understand the physical significance of this stability criterion, consider a linear, one degree of freedom system where $n = 1$. When $n = 1$, inequality (23) reduces to inequality (24).

$$|H| < \left| \frac{(S+1/E)}{G} \right| \text{ for all } \omega \in (0, \infty) \quad (24)$$

where $| \cdot |$ denotes the magnitude of transfer function.⁹ Since in many cases $G \approx 1$ for all $0 < \omega < \omega_0$, then H must be chosen such that:

$$|H| < |(S+1/E)| \text{ for all } \omega \in (0, \omega_0) \quad (25)$$

where ω_0 is the closed-loop bandwidth. The smaller the sensitivity of the robot manipulator, the smaller H must be. Also from inequality (25), the more rigid the environment is, the smaller H must be. In the "ideal case" when the robot is a perfect positioning system ($S=0$), no H can be found to enable interaction with an infinitely rigid environment

⁸The maximum singular value of a matrix A , $\sigma_{\max}(A)$ is defined as:

$$\sigma_{\max}(A) = \max \frac{|Az|}{|z|}$$

where z is a nonzero vector and $| \cdot |$ denotes the Euclidean norm.

⁹The maximum singular values reduce to $| \cdot |$ for a one-dimensional system.

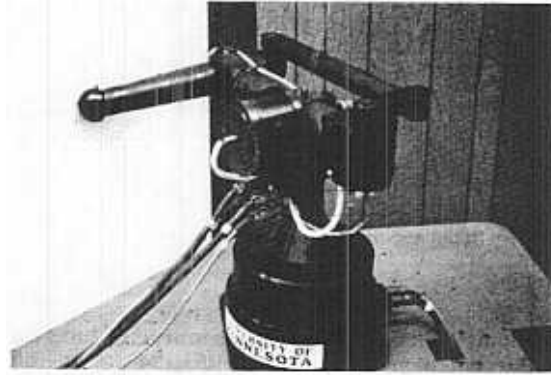


Fig. 6 University of Minnesota robot

($E \rightarrow \infty$). In other words, for stability of the system shown in Fig. 5, there must be some compliancy either in the robot or in the environment. The robot compliancy may be due to an RCC, structural flexibility, and/or the electronic compliancy resulting from the tracking controller.¹⁰ Direct drive manipulators, because of the elimination of the transmission systems, can potentially have large S . This allows for a wider stability range in constrained manipulation. References [1 and 20] are examples of two control methodologies that result in nonzero sensitivity for the robot.

This result can also be extended to nonlinear multivariable systems. When the robot interacts with a very stiff environment, the small size of the environment deflection, $x \approx 0$ results in $y \approx x_0$. Equation (10) may be rewritten as:

$$G(e) + S(-f) = x_0 \quad (26)$$

If the closed-loop position controller is designed such that $G \approx I_n$ then:

$$f = -S^{-1}(x_0 - e) \quad (27)$$

where S^{-1} is the inverse function of S . Recall that V is defined as a mapping from e to f . When the environment is infinitely stiff, one can use S^{-1} in equation (27) as a mapping from e to f for a given x_0 . In other words, for an infinitely stiff environment, the operator V is the same as inverse of the sensitivity function of the robot. This indicates that to satisfy the nonlinear stability condition (inequality 22), the "size" of H must be smaller than the "size" of the robot sensitivity. This is similar to the result given for linear systems. We use this concept in our experimental analysis where the stability condition has been verified in several constrained maneuvers.

5 Structured Modeling

To evaluate the nonlinear stability condition, a compliance controller was implemented on the University of Minnesota robot (Fig. 6), a statically balanced, direct-drive, three-degree-

¹⁰When the environment is very stiff, (E is very "large" in the singular value sense), the limiting value for the contact force and stability condition for all $\omega \in (0, \omega_0)$, are given by the following equations, respectively:

$$f_{\infty} = (S+GH)^{-1}r$$

$$\sigma_{\max}(H) < \sigma_{\min}(S) \text{ for all } \omega \in (0, \omega_0)$$

By knowing S and choosing H , one can shape the contact force. The value of $(S+H)$ within $(0, \omega_0)$ is the designer's choice and, depending on the task, it can have various values in different directions (8). A large value for $(S+H)$ within $(0, \omega_0)$ develops a compliant system while a small $(S+H)$ generates a stiff system. By inspection of the stability condition, it is clear that if the environment is very rigid, then one must choose a very small H to satisfy the stability of the system when S is "small." Direct drive manipulators, because of the elimination of the transmission systems, often have large S . This allows for a wider stability range in constrained manipulation.

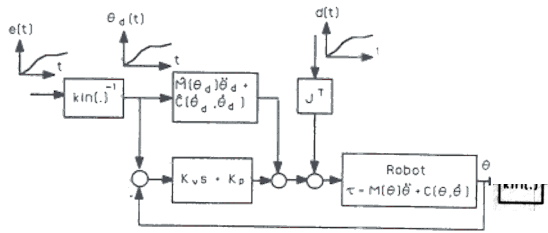


Fig. 7 Robot and feedforward torque controller dynamics [1, 2]

of-freedom robot which was constructed to evaluate nonlinear, compliance control algorithms [9, 10]. Because this robot does not contain any gearing, frictional losses are small and consequently the manipulator can be modeled by equation (28).

$$M(\theta)\ddot{\theta} + C(\theta, \dot{\theta}) = \tau + J^T d \quad (28)$$

where $\ddot{\theta}$, $\dot{\theta}$, θ are vectors containing the joints' accelerations, velocities, and positions, respectively; $M(\theta)$ is the inertia matrix; $C(\theta, \dot{\theta})$ is the vector representing the coriolis, centrifugal and gravity forces, τ , is the vector of joint torques, J^T is the Jacobian transpose matrix, and d is the vector of external forces applied at the robot end-point. Because of the statically balanced construction, gravity does not appear in the robot dynamics. The $M(\theta)$ and $C(\theta, \dot{\theta})$ functions for the University of Minnesota Robot have been computed in closed form and the coefficients for these functions have been experimentally identified [10].

Trajectory control for the manipulator is performed by a digital implementation of a feedforward torque controller, which is given by:

$$\tau = K_p(\theta_d - \theta) + K_v(\dot{\theta}_d - \dot{\theta}) + \hat{M}(\theta_d)\ddot{\theta}_d + \hat{C}(\theta_d, \dot{\theta}_d) \quad (29)$$

where τ is the vector of joint torques; $(\theta_d - \theta)$ is the error between the command position, θ_d , and the actual position, θ , and $(\dot{\theta}_d - \dot{\theta})$ is the error between the respective velocities; K_p is a 3×3 diagonal matrix containing the position gains; K_v is a 3×3 diagonal matrix containing the velocity gains; $\hat{M}(\theta_d)$ is the experimentally identified, inertia matrix; and $\hat{C}(\theta_d, \dot{\theta}_d)$ is the experimentally identified, 3×1 vector of centrifugal and coriolis forces. The physical reasoning behind this control law is that the nonlinear feedforward terms, $\hat{M}(\theta_d)$ and $\hat{C}(\theta_d, \dot{\theta}_d)$, tend to cancel the effects of nonlinear effects of $M(\theta)$ and $C(\theta, \dot{\theta})$ in the robot's dynamics and result in a nearly uncoupled, linear system. The feedforward controller and robot dynamics are shown in Fig. 7. In feedforward torque control, the robot trajectory is specified in joint coordinates, and the joint positions, velocities, and accelerations for a given trajectory are computed and stored before the trajectory is executed. The $Kin(\cdot)$ operator in the diagram represents the forward kinematics, while $Kin^{-1}(\cdot)$ represents the inverse kinematics. When the trajectory is specified in cartesian space as a function of time, $e(t)$, the inverse kinematics and numerical differentiation are employed to transform it into joint space, $\theta_d(t)$.

The nonlinear control law of equation (29) was chosen because the inertia and coriolis terms could be computed and stored. During the trajectory execution, these terms were added to the error terms to compute the joint torques. The chief advantage of this approach is that only a modest amount of computation must be performed in real time, and the sampling time is correspondingly reduced. The shorter sampling time reduces the time delay associated with the digital controller's sample and hold and, consequently, reduces the discrete-time influence on a controller designed for continuous time.

Although feedforward torque control is computationally efficient, the method does not achieve perfect uncoupling of

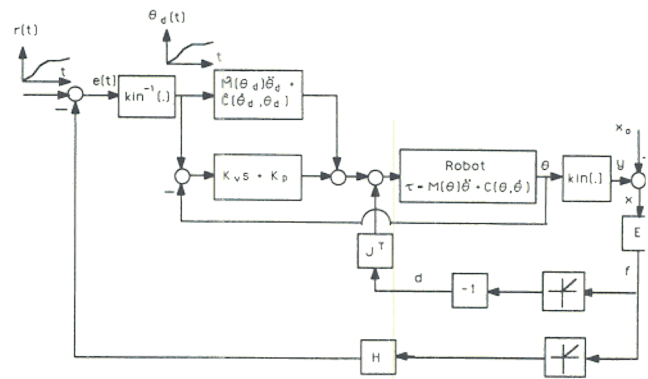


Fig. 8 Trajectory controller, robot dynamics, environment dynamics, and compliance compensator. This block diagram has the same structure as the one in Figure 3.

each joint. Using equations (28) and (29) and assuming that $\hat{C}(\theta_d, \dot{\theta}_d) \approx C(\theta, \dot{\theta})$ and $\hat{M}(\theta_d) \approx M(\theta)$, a differential equation in terms of the joint accelerations is obtained:

$$\ddot{\theta} = \ddot{\theta}_d + M(\theta)^{-1}(K_p(\theta_d - \theta) + K_v(\dot{\theta}_d - \dot{\theta})) - M(\theta)^{-1}J^T f \quad (30)$$

where $M(\theta)$ is a symmetric, positive definite matrix whose inverse exists for all possible robot configurations, θ . Note that despite the assumption that the robot dynamics are accurately known, the joints are not perfectly uncoupled, and the degree of coupling varies as a function of the configuration.

In addition, with this robot control system, the output, θ , is a function of both the command trajectory, θ_d , and the external force, f . The relationship between the inputs and outputs, for the feedforward torque law, are nonlinear mappings. Applying the definitions of the G : $e(t) \rightarrow y(t)$ and S : $f(t) \rightarrow y(t)$ mappings, the respective differential equations are:

$$\dot{\theta}_d(t) = kin^{-1}(e(t)) \quad (31)$$

$$M(\theta)(\ddot{\theta} - \ddot{\theta}_d) = [K_p(\theta_d - \theta) + K_v(\dot{\theta}_d - \dot{\theta})] - J^T(\theta)f \quad (32)$$

$$y(t) = kin[\theta(t)] \quad (33)$$

Equations (31)–(33) contain the nonlinear matrix functions $M(\theta)$ and $J^T(\theta)$, therefore G and S are nonlinear mappings. Figure 8 shows the system architecture when the robot interacts with the environment and the robot compliancy is tailored by means of an H compensator. The product of the environment mapping, E , is an external force, f , which is expressed in the global cartesian coordinate frame. Although the trajectory controller operates in the manipulator joint space, H has been implemented as linear transfer function which can accept the cartesian force and produce a cartesian displacement. The product of H is a small displacement. In practice, $r(t)$ is transformed into joint space prior to execution; the inverse Jacobian, J^{-1} , is substituted for $kin^{-1}(\cdot)$ in the system.

6 Structured Control and Stability Analysis

Some experiments have been performed to demonstrate that inequality (22) is a sufficient condition for stability: one in which the satisfaction of the condition leads to a stable maneuver and one in which parameters for an unstable maneuver violate the condition. For a sufficient stability condition, recall that if the condition is satisfied, the stability is guaranteed; however, if the condition is violated, no conclusion can be made. In the first experiment, we design an H such that inequality (22) is satisfied and show, through experiment, that the system is stable. In the second experiment, we show that an H which destabilizes the system also violates inequality (22).

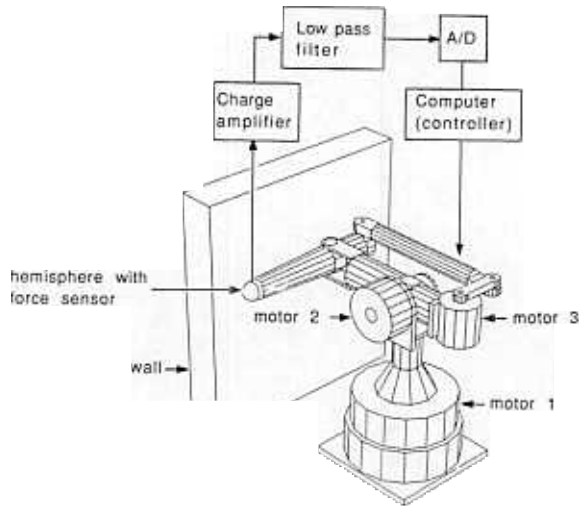


Fig. 9 The experimental setup

In order to find a stability bound on H , we must determine the operator, $V: e(t) \rightarrow f(t)$, for the robot controller. To determine the greatest bound on V , we assume that the wall is very stiff, such that $y \approx x_0$. In this case, one can use the gain of the S^{-1} (equation (27)) to calculate α_1 , as opposed to equations (31)–(33). The “worst case” stability condition can be attributed to the case where the robot is constrained by an infinitely rigid environment in all directions and therefore $(\hat{\theta}_d - \hat{\theta}) = (\theta_d - \theta) = 0$. Equation (32), under the above condition, can be written as:

$$J^T(\theta)f = k_p(\theta_d - \theta) \quad (34)$$

Substituting for θ_d and θ from equations (31) and (33) into equation (34) results in equation (35).

$$J^T(\theta)f = K_p[kin^{-1}(e) - kin^{-1}(y)] \quad (35)$$

Since the wall is very stiff, substituting $y \approx x_0$ in equation (35) results in:

$$f = J^{-T}K_p[kin^{-1}(e) - kin^{-1}(X_0)] \quad (36)$$

We assume that the trajectory, e , commands the robot to maneuver only a small distance beyond the solid wall. This is of paramount importance in practice because large values of $e - x_0$ result in large contact forces. Since $e - x_0$ is a small quantity, $kin^{-1}(e) - kin^{-1}(x_0)$ can be replaced by $J^{-1}(e - x_0)$.

$$f = J^{-T}K_pJ^{-1}(e - x_0) \quad (37)$$

Comparing equation (27) with (37) shows that $J^{-T}K_pJ^{-1}$ is, in fact, the inverse of the sensitivity function. Using inequality (22), the stability condition is:

$$\gamma < \frac{1}{\alpha_1} \quad (38)$$

where α_1 is the supremum of $\sigma_{\max}(J^{-T}K_pJ^{-1})$ over the commanded trajectory. Equivalently one can satisfy inequality (39)

$$\gamma < \text{infimum of } \sigma_{\min}(JK_p^{-1}J^T) \text{ over the commanded trajectory} \quad (39)$$

One must calculate the minimum singular value of $(JK_p^{-1}J^T)$ at each point in the commanded trajectory. The infimum is the lowest of all the minimum singular values. The gain of H (expressed in terms γ) must be chosen smaller than this infimum. From inequality (39), the stability region will approach zero when the robot maneuvers near singular point ($\det(J) \rightarrow 0$)

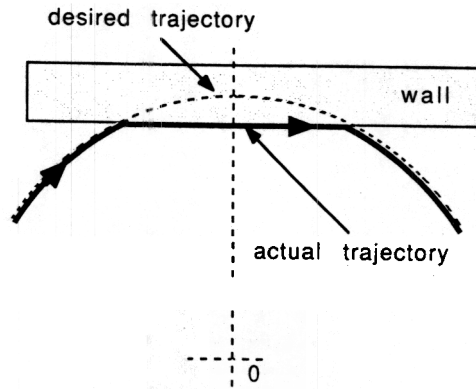


Fig. 10 The top view of the experimental setup. The dashed line is the desired end point trajectory while the solid line is the actual trajectory.

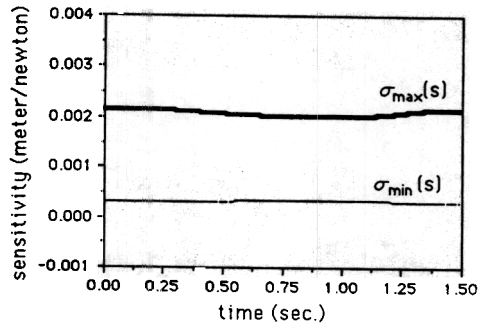


Fig. 11 The maximum and minimum singular values of the sensitivity function for the actual trajectory shown in Fig. 10

and/or when the position gains approach infinity. Both cases are instances of “infinite stiffness” for the robot, the first is due to the robot configuration, while the second is due to the tracking controller.

7 Experimental Results

A reinforced aluminum wall was mounted vertically in the robot workspace as shown in Fig. 9 to simulate a stiff environment. Motor 2 was mechanically locked while motors 1 and 3 were used to actuate the robot for horizontal maneuvering; this resulted in planar, horizontal motion of the robot end-point in global, cartesian space. A force sensor is mounted on the manipulator end-point to measure contact forces. Figure 10 shows the top view of experimental setup. Since the experiments are all two-dimensional, H is a 2×2 matrix operating on contact forces which are normal and tangential to the wall. (The end-point force measurements were resolved into the global coordinate frame.) In these experiments, only the compliancy in the direction normal to the wall was supplemented, so the following form of H was chosen:

$$H = \begin{bmatrix} \frac{H_0}{T} & 0 \\ 0 & 0 \end{bmatrix} \quad (40)$$

where T is empirically chosen constant and is used to filter the high frequency noise in the force measurement. T was fixed at 0.05 for all the experiments to filter the high frequency noise in the force sensor. The function, $r(t)$, shown in Fig. 10 by the dashed line, is chosen as the assigned trajectory to the robot. Since H has only one non-zero member, then γ will be the maximum value of the magnitude of $H_0/(Tj\omega + 1)$. The maximum value of H is H_0 and occurs at DC ($\omega = 0$).

In the first experiment, we show that if inequality (39) is

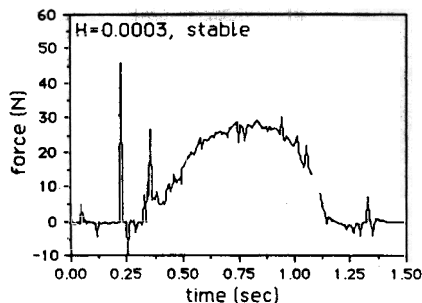


Fig. 12 Experimental measurement of the stable normal contact force. $H_0 = 0.0003$ satisfies the stability condition.

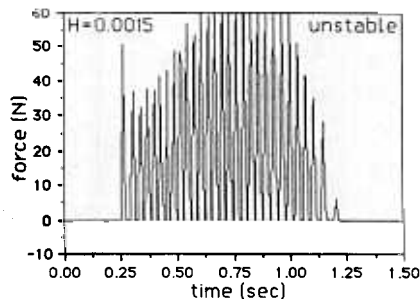


Fig. 15 Simulation of the unstable normal contact force. $H_0 = 0.0015$ does not satisfy the stability condition.

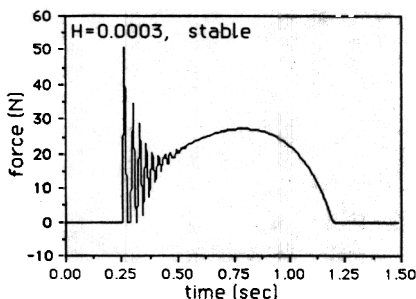


Fig. 13 Simulation of the stable normal contact force. $H_0 = 0.0003$ satisfies the stability condition.

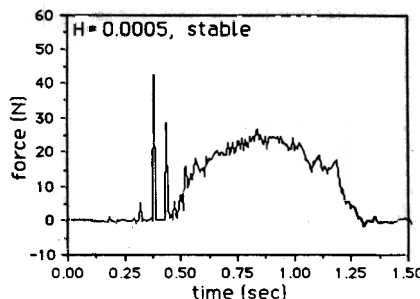


Fig. 16 Experimental measurement of the normal contact force. $H_0 = 0.0005$ violates the stability condition, however the system is stable.

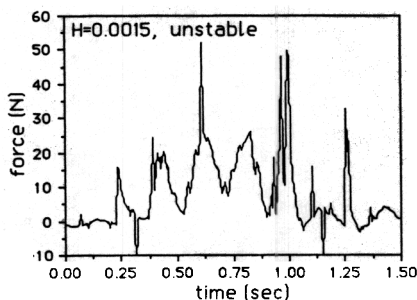


Fig. 14 Experimental measurement of the unstable normal contact force. $H_0 = 0.0015$ does not satisfy the stability condition.

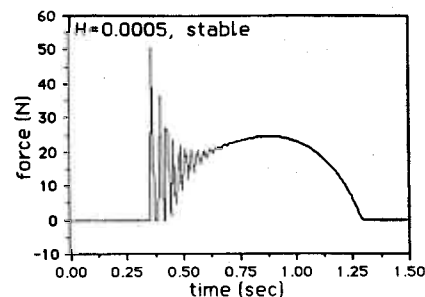


Fig. 17 Simulation of the normal contact force. $H_0 = 0.0005$ violates the stability condition, however the system is stable.

satisfied for a maneuver shown in Fig. 10, then the robot can have stable interaction with the environment. Figure 11 shows the maximum and minimum singular values of $(JK_p^{-1}J^T)$ evaluated for all configurations along the trajectory. We choose H_0 to be .0003 so $H(s)$ was smaller than $\sigma_{\min}(JK_p^{-1}J^T)$ for all configurations within the maneuver. Figs. 12 and 13 show the experimental and simulated values of the normal contact force. The stable contact was indicated by the absence of undamped oscillations in the normal force.

In the second experiment, H_0 was set to .0015. Figures 14 and 15 show the normal contact force as a function of time for experiment and simulation, respectively. In both results, the contact force oscillated throughout the maneuver, indicating that the compliance controller was unstable. Comparison with the singular value plot in Fig. 11, shows that H_0 exceeded the lower bound on $\sigma_{\min}(JK_p^{-1}J^T)$; hence, the stability condition has been violated. Since inequality (39) is only a sufficient condition for stability, violation of this condition does not lead to any conclusion. Figures 16 and 17 show the experimental and simulated contact forces when $H_0 = 0.0005$. The system was stable yet the stability condition was not satisfied.

8 Summary and Conclusion

We have shown how unstructured and structured modeling can be combined to derive a stability condition for a particular robot performing compliant motion. The unstructured model-

ing, which focuses on the input-output characteristics of the system, enables the derivation of a general stability condition. The structured modeling contains the robot and environment dynamics which are specific to a particular robot and controller architecture. We have used this approach to analyze compliant motion on the University of Minnesota robot using a feedforward torque controller and have obtained a stability condition for this application. Through both simulation and experimentation, the sufficiency of this condition has been demonstrated. We have shown that for the stability of the environment and the robot taken as a whole, there must be some initial compliancy either in the robot or in the environment.

APPENDIX A

Definitions 1 to 7 will be used in the stability proof of the closed-loop system [21, 22].

Definition 1: For all $p \in (1, \infty)$, we label as L_p^n the set consisting of all functions $f = (f_1, f_2, \dots, f_n)^T: (0, \infty) \rightarrow \mathbb{R}^n$ such that:

$$\int_0^\infty |f_i|^p dt < \infty \quad \text{or } i = 1, 2, \dots, n$$

Definition 2: For all $T \in (0, \infty)$, the function f_T is defined by:

$$f_T = \begin{cases} f & 0 \leq t \leq T \\ 0 & T < t \end{cases}$$

and f_T is called the truncation of f to the interval $(0, T)$.

Definition 3: The set of all functions $f = (f_1, f_2, \dots, f_n)^T: (0, \infty) \rightarrow \mathbb{R}^n$ such that $f^T \in L^n_p$ for all finite T is denoted by L^n_{pe} . f by itself may or may not belong to L^n_p .

Definition 4: The norm on L^n_p is defined by:

$$\|f\|_p = \left(\sum_{i=1}^n \|f_i\|_p^2 \right)^{1/2}$$

where $\|f_i\|_p$ is defined as:

$$\|f_i\|_p = \left(\int_0^\infty w_i |f_i|^p dt \right)^{1/p}$$

where w_i is the weighting factor. w_i is particularly useful for scaling forces and torques of different units.

Definition 5: Let $v(\cdot): L^n_{pe} \rightarrow L^n_p$. We say that the operator $V(\cdot)$ is L_p -stable, if:

- (a) $v(\cdot): L^n_p \rightarrow L^n_p$
- (b) there exist finite real constants α_1 and β_1 such that:

$$\|v(e)\|_p \leq \alpha_1 \|e\|_p + \beta_1 \quad \forall e \in L^n_p$$

According to this definition we first assume that the operator maps L^n_{pe} to L^n_{pe} . It is clear that if one does not show $v(\cdot): L^n_{pe} \rightarrow L^n_{pe}$, the satisfaction of condition (a) is impossible since L^n_{pe} contains L^n_p . Once mapping, $v(\cdot)$, from L^n_{pe} to L^n_{pe} is established, then we say that the operator $V(\cdot)$ is L_p -stable if, whenever the input belongs to L^n_p , the resulting output belongs to L^n_p . Moreover, the norm of the output is not larger than α_1 times the norm of the input plus the offset constant β_1 .

Definition 6: The smallest α_1 such that there exists a β_1 so that inequality b of Definition 5 is satisfied is called the gain of the operator $V(\cdot)$.

Definition 7: Let $V(\cdot): L^n_{pe} \rightarrow L^n_{pe}$. The operator $V(\cdot)$ is said to be casual if:

$$V(e)_T = V(e_T) \quad \forall T < \infty \text{ and } \forall e \in L^n_{pe}$$

Proof of the nonlinear stability proposition

Define the closed-loop mapping $A: r \rightarrow e$ (Fig. 3).

$$e = r - H(V(e)) \quad (A1)$$

For each finite T , inequality (A2) is true.

$$\|e_T\|_p \leq \|r_T\|_p + \|H(V(e))_T\|_p \quad \text{for all } t \in (0, T) \quad (A2)$$

Since $H(V(e))$ is L_p -stable, inequality (A3) is true.

$$\|e_T\|_p \leq \|r_T\|_p + \alpha_2 \alpha_1 \|e_T\|_p + \alpha_2 \beta_1 + \beta_2 \quad \text{for all } t \in (0, T) \quad (A3)$$

Since $\alpha_5 \alpha_4$ is less than unity:

$$\|e_T\|_p \leq \frac{\|r_T\|_p}{1 - \alpha_2 \alpha_1} + \frac{\alpha_2 \beta_1 + \beta_2}{1 - \alpha_2 \alpha_1} \quad \text{For all } t \in (0, T) \quad (A4)$$

Inequality (A4) shows that $e(\cdot)$ is bounded over $(0, T)$. Because this reasoning is valid for every finite T , it follows that $e(\cdot) \in L^n_{pe}$, i.e., that $A: L^n_{pe} \rightarrow L^n_{pe}$. Next we show that the mapping A is L_p -stable in the sense of definition 5. Since $r \in L^n_p$, therefore $\|r\|_p < \infty$ for all $t \in (0, \infty)$, therefore inequality (A5) is true.

$$\|e\|_p < \infty \quad \text{for all } t \in (0, \infty) \quad (A5)$$

inequality (A5) implies e belongs to L_p -space whenever r belongs to L_p -space. With the same reasoning from equations (A1) to (A5), it can be shown that inequality (A6) is true.

$$\|e\|_p \leq \frac{\|r\|_p}{1 - \alpha_2 \alpha_1} + \frac{\alpha_2 \beta_1 + \beta_2}{1 - \alpha_2 \alpha_1} \quad \text{for all } t \in (0, \infty) \quad (A6)$$

Inequality (A6) shows the linear boundedness of e (condition b of definition 5). Inequalities (A6) and (A5) taken together, guarantee that the closed-loop mapping A is L_p -stable.

APPENDIX B

The block diagram in Fig. 3 can be reduced to the block diagram in Fig. B1 when all the operators are linear transfer function matrices and $x_0 = 0$.

There are two elements in the feedback loop; GHE and SE . SE shows the natural force feedback while GHE represents the controlled force feedback in the system. If $H=0$, then the system in Fig. B1 reduces to the system in Fig. 2 (a stable positioning robot manipulator which is in contact with the environment E .) The objective is to use Nyquist Criterion to arrive at the sufficient condition for stability of the system when $H \neq 0$. The following conditions are assumed [15]:

1) The closed-loop system in Fig. B1 is stable if $H=0$. This condition simply states the stability of the robot manipulator and environment when they are in contact.

2) H is chosen as a stable linear transfer function matrix. Therefore the augmented loop transfer function ($GHE + SE$) has the same number of unstable poles that SE has. Note that in many cases SE is a stable system.

3) Number of poles on $j\omega$ axis for both loops SE and ($GHE + SE$) are equal.

Considering that the system in Fig. B1 is stable when $H=0$, we plan to find how robust the system is when GHE is added to the feedback loop. If the loop transfer function SE (without compensator, H) develops a stable closed-loop system, then we are looking for a condition on H such that the augmented loop transfer function ($GHE + SE$) guarantees the stability of the closed-loop system. According to the Nyquist Criterion, the system in Fig. B1 remains stable if the counter clockwise encirclement of the $\det(SE + GHE + I_n)$ around the center of the s -plane is equal to the number of unstable poles of the loop transfer function ($GHE + SE$). According to conditions 2 and 3, the loop transfer functions SE and ($GHE + SE$) both have the same number of unstable poles. The closed-loop system when $H=0$ is stable according to condition 1; the encirclements of $\det(SE + I_n)$ are equal to the unstable poles of SE . When GHE is added to the system, for stability of the closed-loop system, the number of the encirclements of $\det(SE + GHE + I_n)$ must be equal to the number of unstable poles of ($GHE + SE$). Since the number of unstable poles of ($SE + GHE$) and SE are the same, the stability of the system $\det(SE + GHE + I_n)$ must have the same number of encirclements that $\det(SE + I_n)$ has. A sufficient condition to guarantee the equality of the number of encirclements of $\det(SE + GHE + I_n)$ and $\det(SE + I_n)$ is that the

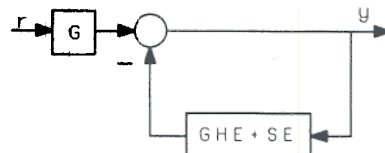


Fig. B1 Simplified block-diagram of the system in Fig. 3

$\det(SE + GHE + I_n)$ does not pass through the origin of the s -plane for all possible non-zero but finite values of H , or

$$\det(SE + GHE + I_n) \neq 0 \quad \text{for all } \omega \in (0, \infty) \quad (\text{B1})$$

If inequality B1 does not hold then there must be a non-zero vector z such that:

$$(SE + GHE + I_n)z = 0 \quad (\text{B2})$$

or:
$$GHE z = -(SE + I_n)z \quad (\text{B3})$$

A sufficient condition to guarantee that equality (B3) will not happen is given by inequality (B4).

$$\sigma_{\max}(GHE) < \sigma_{\min}(SE + I_n) \quad \text{for all } \omega \in (0, \infty) \quad (\text{B4})$$

Similar to steps (B1) through (B4) and isolating H , a more conservative condition is given by (B5):

$$\sigma_{\max}(H) < \frac{1}{\sigma_{\max}(E(SE + I_n)^{-1}G)} \quad \text{for all } \omega \in (0, \infty) \quad (\text{B5})$$

Note that $E(SE + I_n)^{-1}G$ is the transfer function matrix that maps e to the contact force, f . Figure 5 shows the the closed-loop system. According to the result of the proposition, H must be chosen such that the size of H is smaller than the reciprocal of the size of the forward loop transfer function, $E(SE + I_n)^{-1}G$.

APPENDIX C

The following inequalities are true when $p=2$ and H and V are linear operators.

$$\|H(V(e))\|_p \leq \nu \|V(e)\|_p \quad (\text{C1})$$

$$\|V(e)\|_p \leq \mu \|e\|_p \quad (\text{C2})$$

where

$\mu = \sigma_{\max}(Q)$, and Q is the matrix whose ij th entry is given by $(Q)_{ij} = \sup_{\omega} |(V)_{ij}|$,

$\nu = \sigma_{\max}(R)$, and R is the matrix whose ij th entry is given by $(R)_{ij} = \sup_{\omega} |(H)_{ij}|$

Substituting inequality (C2) in (C1):

$$\|HV(e)\|_p \leq \mu \nu \|e\|_p \quad (\text{C3})$$

According to the stability condition, to guarantee the closed loop stability $\mu \nu < 1$ or:

$$\nu < \frac{1}{\mu} \quad (\text{C4})$$

Note that the followings are true:

$$\sigma_{\max}(V) \leq \mu \quad \text{for all } \omega \in (0, \infty) \quad (\text{C5})$$

$$\sigma_{\max}(H) \leq \nu \quad \text{for all } \omega \in (0, \infty) \quad (\text{C6})$$

Substituting (C5) and (C6) into inequality (C4) which guarantees the stability of the system, the following inequality is obtained:

$$\sigma_{\max}(H) < \frac{1}{\sigma_{\max}(V)} \quad \text{for all } \omega \in (0, \infty) \quad (\text{C7})$$

$$\sigma_{\max}(H) < \frac{1}{\sigma_{\max}(E(I_n + SE)^{-1}G)} \quad \text{for all } \omega \in (0, \infty) \quad (\text{C8})$$

Inequality (C8) is identical to inequality (23). This shows that the linear condition for stability given by the multivariable Nyquist Criterion is a subset of the general condition given by the Small Gain Theorem.

References

- 1 An, C. H., and Hollerbach, J. M., "Dynamic Stability Issues in Force Control of Manipulators," IEEE International Conference on Robotics and Automation, Raleigh, NC, Mar. 1987.
- 2 Craig, J. J., *Adaptive Control of Mechanical Manipulators*, Addison-Wesley, Reading, MA, 1988.
- 3 Colgate, J. E., and Hogan, N., "Robust Control of Dynamically Interacting Systems," *International Journal of Control*, Vol. 48, No. 1, July 1988.
- 4 Hogan, N., "Impedance Control: An Approach to Manipulation," ASME JOURNAL OF DYNAMIC SYSTEMS, MEASUREMENT, AND CONTROL, 1985.
- 5 Hogan, N., "On the Stability of Manipulators Performing Constrained Tasks," *IEEE Journal of Robotics and Automation*, No. 6, Vol. 4, Dec. 1988.
- 6 Kazerooni, H., Houpt, P. K., "On the Loop Transfer Recovery," *International Journal of Control*, Vol. 43, No. 3, Mar. 1986.
- 7 Kazerooni, H., "An Approach to Automated Deburring by Robot Manipulators," ASME JOURNAL OF DYNAMIC SYSTEMS, MEASUREMENT AND CONTROL, Dec. 1986.
- 8 Kazerooni, H., "Direct Drive Active Compliant End-Effector," *IEEE Journal of Robotics and Automation*, Vol. 4, No. 3, June 1988.
- 9 Kazerooni, H., and Kim, S., "A New Architecture for Direct Drive Robots," *IEEE International Conference on Robotics and Automation*, Vol. 1, Philadelphia, PA, Apr. 1988, pp. 442-445.
- 10 Kazerooni, H., and Kim, S., "Statically-Balanced Direct Drive Robot for Compliance Control Analysis," ASME Winter Annual Meeting, *Modeling and Control of Robotic Manipulators and Manufacturing Process*, DSC, Vol. 6, Dec. 1987, pp. 193-201, Boston, MA.
- 11 Kazerooni, H., "Fundamentals of Robust Compliant Motion for Manipulators," *IEEE Journal of Robotics and Automation*, Vol. 2, No. 2., June 1986.
- 12 Kazerooni, H., "A Design Method for Robust Compliant Motion of Manipulators," *IEEE Journal of Robotics and Automation*, No. 2, Vol. 2, June 1986.
- 13 Kazerooni, H., Tsay, T. I., "On the Stability of the Constrained Robotic Maneuver," American Control Conference, Atlanta, Georgia, June 1988.
- 14 Lancaster, P., *Lambda-Matrices and Vibrating Systems*, Pergamon Press, 1966.
- 15 Lehtomaki, N. A., Sandell, N. R., Athans, M., "Robustness Results in Linear-Quadratic Gaussian Based Multivariable Control Designs," *IEEE Transaction on Automatic Control* AC-26(1):75-92, Fig. 1981.
- 16 Mason, M. T., "Compliance and Force Control for Computer Manipulators," *IEEE Transaction on Systems, Man, and Cybernetics* SMC-11(6): June 1981, pp. 418-432.
- 17 Paul, R. P. C., Shimano, B., "Compliance and Control," *Proceedings of the Joint Automatic Control Conference*, San Francisco, 1976, pp. 694-699.
- 18 Raibert, M. H., and Craig, J. J., "Hybrid Position/Force Control of Manipulators," ASME JOURNAL OF DYNAMIC SYSTEMS, MEASUREMENT, AND CONTROL, Vol. 102, June 1981, pp. 126-133.
- 19 Salisbury, K. J., "Active Stiffness Control of Manipulator in Cartesian Coordinates," *Proceedings of the 19th IEEE Conference on Decision and Control*, IEEE, Albuquerque, New Mexico, Dec. 1980, pp. 95-100.
- 20 Shin, K. G., and Lee, C.-P., "Compliant Control of Robotic Manipulators with Resolved Acceleration," IEEE Conference on Decision and Control, Ft. Lauderdale, Dec. 1985.
- 21 Vidyasagar, M., *Nonlinear Systems Analysis*, Prentice-Hall, 1978.
- 22 Vidyasagar, M., and Desoer, C. A., *Feedback Systems: Input-Output Properties*, Academic Press, 1975.
- 23 Vidyasagar, M., Spong, M. W., "Robust Nonlinear Control of Robot Manipulators," IEEE Conference on Decision and Control, Dec. 1985.
- 24 Whitney, D. E., "Force-Feedback Control of Manipulator Fine Motions," ASME JOURNAL OF DYNAMIC SYSTEMS, MEASUREMENT, AND CONTROL, June 1977, pp. 91-97.